The Astrophysical Journal, 659:1420–1430, 2007 April 20

LOW-LUMINOSITY GRB 060218: A COLLAPSAR JET FROM A NEUTRON STAR, LEAVING A MAGNETAR AS A REMNANT?

Kenji Toma,[1] Kunihito Ioka,[1] Takanori Sakamoto,[2,3] and Takashi Nakamura[1]
Received 2006 October 30; accepted 2006 December 30

ABSTRACT

The gamma-ray burst (GRB) 060218 has a luminosity $\sim 10^5$ times lower than that of typical long GRBs and is associated with a supernova (SN). The radio afterglow displays no jet break, so this burst might arise from a mildly relativistic spherical outflow produced by the SN shock sweeping the stellar surface. Since this model is energetically difficult, we propose that the radio afterglow is produced by a nonrelativistic phase of an initially collimated outflow (jet). Our jet model is supported by the detection of optical linear polarization in the SN component. We also show analytically that the jet can penetrate a progenitor star. We analyzed the observational data of the prompt emission of this burst and obtained a smooth power-law light curve which might last longer than 10^6 s. This behavior contrasts with the long intermittent activities of the X-ray flares of typical GRBs, implying that the central engine of this burst is different from those of typical GRBs. This argument is consistent with the analysis of the SN component of this burst, which suggests that the progenitor star was less massive and collapsed to a neutron star instead of a black hole. The collimation-corrected event rate of such low-luminosity GRBs is estimated to be ~ 10 times higher than that of typical long GRBs, and they might form a different GRB population: low-luminosity GRBs are produced by mildly relativistic jets from neutron stars at the collapses of massive stars, while typical long GRBs are produced by highly relativistic jets from black holes. We suggest that the central engine of GRB 060218 is a pulsar (or a magnetar) with initial rotation period $P_0 \sim 10$ ms and magnetic field $B \sim 10^{16}$ G. A giant flare from the magnetar might be observed in future.

Subject headings: gamma rays: bursts — gamma rays: theory — supernovae: general

1. INTRODUCTION

The gamma-ray burst (GRB) 060218 is the second nearest event of its kind ($z = 0.033$) and is spectroscopically associated with the supernova (SN) 2006aj (Modjaz et al. 2006; Sollerman et al. 2006; Pian et al. 2006; Mazzali et al. 2006; Mirabal et al. 2006; Cobb et al. 2006; Ferrero et al. 2006). Such a long GRB/SN association is common, and this event further supports the established picture that all long GRBs are related to the deaths of massive stars (for recent reviews, see Woosley & Bloom 2006; Mészáros 2006; Piran 2005; Zhang & Mészáros 2004). In the most popular model of long GRBs, the so-called collapsar model, the core of a massive star collapses to a black hole or a neutron star, which drives a highly relativistic jet, breaking out of the star and making a GRB (Woosley 1993; MacFadyen & Woosley 1999). The relativistic speed of the outflow is required for the nonthermal prompt emission (Lithwick & Sari 2001 and references therein). The collimation of the outflow is strongly suggested by a break in the afterglow, since it is produced by the sideways expansion of the jet (e.g., Rhoads 1999; Sari et al. 1999; Harrison et al. 1999).

However, the prompt and afterglow emission of GRB 060218 have many peculiarities (Campana et al. 2006; Soderberg et al. 2006; Ghisellini et al. 2007; Butler 2006; Liang et al. 2006b):

1. The duration of the prompt nonthermal emission in the high-energy band (15–150 keV) is $\delta t \sim 10^3$ s, and this event is thus one of the longest bursts.

2. The isotropic-equivalent luminosity of the prompt emission is extremely low, $\sim 10^{47}$ erg s^{-1}, which is about 10^5 times lower than those of typical cosmological GRBs. The isotropic-equivalent energy, extrapolated to the 1–10^4 keV band in the central engine frame, is $E_{\gamma,\mathrm{iso}} \simeq 6 \times 10^{49}$ erg.

3. The spectrum of the prompt emission is quite soft compared to those of typical bright GRBs, and the averaged spectral peak energy in the central engine frame is $\simeq$4.9 keV (note that this event obeys the Amati correlation, despite the other peculiarities; see § 2 for more details).

4. Thermal components are detected in the X-ray band at $t \lesssim 10^4$ s and in the UV/optical band at $10^4 \lesssim t \lesssim 10^5$ s, while other GRBs do not exhibit such a clear thermal component.

5. The X-ray, UV/optical, and radio afterglows show chromatic features. The X-ray afterglow (at $t \gtrsim 10^4$ s) decays with a standard temporal slope, but has a spectrum much steeper than those of typical GRB X-ray afterglows. The UV/optical afterglow is quite dim and is dominated by the thermal component and the SN component. Only the radio afterglow seems rather typical and explainable in the standard external shock synchrotron model (Sari et al. 1998; Rees & Mészáros 1992; Paczyński & Rhoads 1993), but does not show a jet break until $t \simeq 22$ days.

Although such a low-luminosity event looks rare, the intrinsic event rate could be very high, $R_{\mathrm{LL}} \sim 10^2$ Gpc^{-3} yr^{-1}, compared with the local rate of typical long GRBs deduced from the BATSE data, $R_{\mathrm{LG}} \sim 1$ Gpc^{-3} yr^{-1} (Soderberg et al. 2006; Pian et al. 2006; Cobb et al. 2006; Liang et al. 2006a; Guetta et al. 2004). For this reason, it has been actively debated whether low-luminosity GRBs form a new GRB population and whether they have intrinsically different outflow mechanisms and emission mechanisms (see Stanek et al. 2006; Ghisellini et al. 2006; Kaneko et al. 2006; Amati et al. 2006; Stratta et al. 2006; Dai et al. 2006; Wang et al. 2006). It has also been argued that the high-energy neutrino background from the low-luminosity GRBs could be comparable to or larger than that from typical long GRBs (Murase et al. 2006; Gupta & Zhang 2006).

[1] Department of Physics, Kyoto University, Kyoto 606-8502, Japan; toma@tap.scphys.kyoto-u.ac.jp.
[2] NASA-Goddard Space Flight Center, Greenbelt, MD 20771; takanori@milkyway.gsfc.nasa.gov.
[3] National Research Council, Washington DC 20418.

For GRB 060218, it has been widely suggested that the outflow is spherical, since the radio afterglow has no jet break (Soderberg et al. 2006; Fan et al. 2006). If this is true, the collapsar model cannot be applied to this event because the outflow becomes nonrelativistic by loading all the matter of a progenitor star. The relativistic spherical outflow might be produced by the outermost parts of the stellar envelope that the SN shock accelerates when propagating through the steep density gradient near the stellar surface (Colgate 1974; Matzner & McKee 1999; Tan et al. 2001). However, Tan et al. (2001) have shown that the energy, $\sim 10^{48}$ erg, is transferred to mildly relativistic material when the SN kinetic energy $E_{\rm SN} \sim 10^{52}$ erg. For GRB 060218, $E_{\rm SN}$ is estimated as $\simeq 2 \times 10^{51}$ erg (Mazzali et al. 2006), so it is quite unlikely that the prompt nonthermal emission with $E_{\gamma,\rm iso} \simeq 6 \times 10^{49}$ erg is produced by this type of outflow (see also Matzner 2003). Li (2006) has also shown that the energy of the thermal components, $\gtrsim 10^{49}$ erg, is too large to be explained by the shock breakout in the underlying SN.

In this paper, we show that GRB 060218 can be produced by the standard collapsar jet model. We show that the available radio data may be interpreted as a nonrelativistic phase of the external shock *after the jet break* within the standard model (e.g., Frail et al. 2000; Livio & Waxman 2000). We argue that the outflow with an initial opening angle $\theta_0 \simeq 0.3$ and Lorentz factor $\Gamma_0 \simeq 5$ can produce the synchrotron radiation, explaining the radio afterglow and compatible with the UV/optical and X-ray afterglow (§ 3). We also examine whether such a wide and weak jet can penetrate a progenitor star, by extending analytical considerations of the collapsar model by Matzner (2003; see § 4).

Remarkably, the detection of optical linear polarization in the SN component of this event has recently been reported (Gorosabel et al. 2006). This observation strongly supports our arguments that GRB 060218 arises from a jet.

Within the jet scenario, there is a possibility that low-luminosity GRBs arise as typical cosmological GRB jets viewed off-axis (e.g., Yamazaki et al. 2003; Ramirez-Ruiz et al. 2005; Granot et al. 2005; Toma et al. 2005). The relativistic jet emits γ-rays into the expansion direction through the beaming effect. Thus, if the jet is viewed off-axis, the γ-ray flux is strongly suppressed. This scenario leads to similar event rates for typical GRBs and low-luminosity GRBs, which seems inconsistent with the observations (Cobb et al. 2006). Aside from this statistical argument, we also examine the off-axis scenario for GRB 060218 and conclude that this scenario is unlikely for this event because an unrealistically high γ-ray efficiency is required.

In addition, we analyzed the data of the Burst Alert Telescope (BAT; Barthelmy et al. 2005) and the X-Ray Telescope (XRT; Burrows et al. 2005b) of the *Swift* satellite (Gehrels et al. 2004). We found that the nonthermal component of the prompt emission of GRB 060218 may be fitted by the Band function with spectral parameters similar to those of typical GRBs. Furthermore, we found that the light curve of the nonthermal component evolves smoothly as a power-law function of time and might have so long a duration as to connect to the anomalous X-ray afterglow detected up to $\sim 10^6$ s. This behavior contrasts with the long intermittent activities of the X-ray flares of typical GRBs, which might be a sign of the difference of the central engines. This is also suggested by the analysis of the SN component of this event. The SN spectrum has less broad lines than those of other GRB-SNe and lacks oxygen lines, and the light curve evolves somewhat faster. All of these facts indicate that the total kinetic energy $E_{\rm SN}$ and the ejected mass $M_{\rm ej}$ are both less than those of other GRB-SNe. Mazzali et al. (2006) performed a detailed modeling of the spectra and light curve of the SN component and obtained $E_{\rm SN} \simeq 2 \times 10^{51}$ erg and $M_{\rm ej} \simeq 2\ M_\odot$. They then suggested that the progenitor star of this burst was less massive than those of typical long GRBs and collapsed to a neutron star instead of a black hole.

Our goal is to show that the low-luminosity GRB 060218 has a prompt nonthermal emission with a typical Band spectrum and may originate from a standard collapsar jet, possibly driven by a neutron star. We do not discuss the emission mechanism of the prompt nonthermal emission and the thermal emissions. This paper is organized as follows. In § 2, we show the results of our analysis of the BAT and XRT data and suggest several implications for the nature of the prompt nonthermal emission. In § 3, we display a jet model of this event, discussing whether the jet can make a hole in the star in § 4. A summary and discussion are given in § 5. Since GRB 060218 is very close ($z = 0.033$), we neglect the cosmological effect, i.e., we set $z = 0$ for simplicity throughout this paper.

2. THE PROMPT NONTHERMAL EMISSION

2.1. *BAT and XRT Data Analysis*

We analyzed the BAT and XRT data using the standard *Swift* software package (HEAsoft 6.0.4) and the CALDB 2005-11-28. The detector plane histogram (DPH) data were used to extract the spectra of BAT. Before producing the spectra, we applied `baterebin` to rebin the DPH data using the most accurate nonlinear energy correction. The detector map for disabling noisy detectors in the analysis was created by `bathotpix`. The mask-weighting map was created by `batmaskwtimg` using the optical afterglow position. By including the detector map and the mask-weighting map in `batbinevt`, 13 BAT spectra were extracted from the DPH file containing the data just after the spacecraft slew. The BAT response matrices were generated by `batdrmgen`. The systematic error vectors were applied to the BAT spectra using `batphasyserr`. For the XRT data, we obtained the cleaned event file in the window timing (WT) mode from the *Swift* HEASARC Archive. The foreground was excluded by the box region of $1.2' \times 0.6'$. The background region was extracted by the same region size, but outside of the foreground source region. Thirteen XRT foreground and background spectra using the same time intervals of the BAT spectra were extracted. The auxiliary response file was generated by `xrtmkarf`. The XRT spectra were binned to contain a minimum of 20 photons for each spectral bin.

The XRT and BAT spectral data were analyzed jointly with XSPEC 11.3.2. The energy ranges used in the analysis were 0.5–10 keV and 14.0–150 keV for XRT and BAT, respectively. We multiplied the constant factor to the spectral model to take into account the calibration uncertainty in the response matrices of the instruments. As reported by several authors (Kaneko et al. 2006; Campana et al. 2006; Butler 2006; Liang et al. 2006b), the blackbody component was necessary in order to obtain a good fit for the low-energy part of the XRT spectrum. Thus, we performed the fitting with an additional blackbody (BB) component to an absorbed Band function and an absorbed power-law times exponential cutoff (CPL) model. For the purpose of this paper, we are interested in the spectral parameters of the nonthermal component. To obtain the well-constrained spectral parameters of the nonthermal component, we fixed the parameters of the absorption ($N_{\rm H}$) and the BB component to their best-fit values for each fit, and then calculated the uncertainties of the spectral parameters of the nonthermal component. The results are shown in Tables 1 and 2. Most of the spectra were well fitted by an absorbed CPL model with an additional BB component, as reported by Kaneko et al. (2006) and Campana et al. (2006). However, we

TABLE 1
Spectral Parameters of the Nonthermal Component of GRB 060218 (1)

t (s)	Time Width (s)	α_B	β_B	E_p (keV)	χ^2	dof	$F_{15-150\mathrm{keV}}$ (10^{12} erg cm^{-2} s^{-1})
219.5	81.5	$-1.25^{+0.05}_{-0.05}$	$-3.8^{+1.9}_{-6.2}$	34^{+14}_{-19}	232.7	292	5170^{+640}_{-640}
332.0	30.0	$-1.47^{+0.08}_{-0.07}$	-8.4	23^{+8}_{-6}	156.7	190	6650^{+1020}_{-990}
449.0	45.0	$-1.08^{+0.06}_{-0.06}$	$-2.1^{+0.2}_{-0.2}$	11^{+19}_{-3}	239.4	297	9370^{+310}_{-320}
554.0	60.0	$-1.05^{+0.05}_{-0.05}$	$-2.4^{+0.2}_{-0.3}$	10^{+5}_{-2}	287.8	385	5400^{+210}_{-120}
674.0	60.0	$-1.07^{+0.07}_{-0.06}$	$-2.8^{+0.3}_{-0.6}$	13^{+4}_{-4}	391.4	403	4870^{+510}_{-360}
794.0	60.0	$-1.04^{+0.05}_{-0.05}$	$-2.6^{+0.3}_{-0.4}$	9^{+3}_{-2}	390.7	409	3400^{+170}_{-150}
914.0	60.0	$-1.07^{+0.06}_{-0.04}$	$-2.5^{+0.3}_{-0.4}$	$6.5^{+1.1}_{-1.5}$	388.5	429	3450^{+160}_{-230}
1114.0	140.0	$-1.17^{+0.06}_{-0.03}$	$-3.0^{+0.2}_{-0.9}$	$5.5^{+0.4}_{-0.6}$	629.0	573	1903^{+52}_{-66}
1404.0	150.0	$-1.31^{+0.10}_{-0.04}$	$-4.0^{+0.8}_{-5.2}$	$3.7^{+0.3}_{-0.2}$	576.8	546	890^{+17}_{-10}
1704.5	150.5	$-1.1^{+0.2}_{-0.2}$	$-2.6^{+0.2}_{-0.2}$	$2.6^{+0.1}_{-0.1}$	438.9	486	830^{+330}_{-140}
2005.0	150.0	$-1.1^{+0.5}_{-0.2}$	$-2.6^{+0.1}_{-0.1}$	$2.1^{+0.1}_{-0.1}$	408.6	437	590^{+110}_{-100}
2305.0	150.0	$-1.1^{+0.5}_{-0.5}$	$-2.53^{+0.05}_{-0.05}$	$1.3^{+0.2}_{-1.2}$	375.8	393	563^{+72}_{-106}
2593.5	138.5	$-1.0^{+0.5}_{-0.4}$	$-2.8^{+0.1}_{-0.1}$	$1.6^{+0.1}_{-0.6}$	300.9	344	303^{+63}_{-98}

Notes.—These values are calculated from the joint fit of the BAT and XRT data by the absorbed band function plus the blackbody function. Errors are for 90% confidence.

found a significant improvement in a fit with the Band function for the last four time intervals from 1550 to 2732 s after the BAT trigger. The differences in χ^2 between the CPL and Band fit were 9.6, 11.7, 17.0, and 13.8 in 1 degree of freedom for these spectra. Based on this result, we decided to adopt the spectral parameters derived by the Band function for all time intervals. The temperature of the BB component varies slightly between 0.12 and 0.29 keV. This behavior is consistent with the results of the other analyses (Kaneko et al. 2006; Campana et al. 2006; Butler 2006).

Figure 1 shows the result of the temporal variations of the low-energy and high-energy photon indices, α_B and β_B. Figure 2 shows the light curve in the 15–150 keV band and the spectral peak energy E_p as functions of time. At the flux decay phase ($t \gtrsim 500$ s), the light curve and spectral peak energy are well described by power-law functions of time, $F \propto t^{-2.0}$ and $E_p \propto t^{-1.6}$ (*dotted lines*).

Investigating the consistency of the BAT light curves presented by us and Campana et al. (2006), we found systematic differences, especially for $t > 1000$ s. Although both of the BAT light curves are based on the joint spectral analysis of the BAT and XRT data, Campana et al. (2006) use the CPL model, while we use the Band function. We noticed that the fluxes of the light curve of Campana et al. (2006) at $t > 1000$ s are in the level of $\sim$10 mcrab. BAT can detect the Crab nebula at a 6 σ level in a 1 s exposure. If the BAT sensitivity can be scaled as a square root of the exposure time (Markwardt et al. 2005), we need an exposure time of $\sim 10^4$ s to detect the 10 mcrab source, assuming the Crab-like spectrum. On the other hand, the fluxes of our light curve are in the level of $\sim$100 mcrab at the late phase. This flux level is reasonable to detect in a $\sim$100 s exposure by BAT. Thus, we believe that there is a systematic error by using the CPL model in the BAT flux calculation presented by Campana et al. (2006). We also believe that this investigation strengthens our conclusion that the Band function is the best represented spectral model of the nonthermal emission of GRB 060218.

TABLE 2
Spectral Parameters of the Nonthermal Component of GRB 060218 (2)

t (s)	Time Width (s)	α_c	E_p (keV)	χ^2	dof
219.5	81.5	$-1.36^{+0.04}_{-0.05}$	36^{+15}_{-8}	230.0	293
332.0	30.0	$-1.46^{+0.08}_{-0.08}$	22^{+8}_{-5}	156.6	191
449.0	45.0	$-1.39^{+0.05}_{-0.05}$	31^{+11}_{-7}	237.8	298
554.0	60.0	$-1.34^{+0.05}_{-0.05}$	22^{+7}_{-5}	293.0	386
674.0	60.0	$-1.18^{+0.06}_{-0.05}$	16^{+4}_{-3}	381.2	404
794.0	60.0	$-1.40^{+0.06}_{-0.06}$	15^{+7}_{-4}	393.2	410
914.0	60.0	$-1.44^{+0.07}_{-0.06}$	12^{+5}_{-3}	400.2	430
1114.0	140.0	$-1.42^{+0.07}_{-0.07}$	$5.7^{+0.8}_{-0.6}$	626.8	574
1404.0	150.0	$-1.38^{+0.09}_{-0.08}$	$3.6^{+0.1}_{-0.2}$	573.9	547
1704.5	150.5	$-1.6^{+0.1}_{-0.1}$	$2.2^{+0.1}_{-0.1}$	448.5	487
2005.0	150.0	$-1.8^{+0.1}_{-0.2}$	$1.1^{+0.2}_{-0.1}$	420.3	438
2305.0	150.0	$-1.9^{+0.1}_{-0.1}$	$0.7^{+0.1}_{-0.1}$	392.8	394
2593.5	138.5	-1.7	0.5	314.7	345

Notes.—These values are calculated from the joint fit of the BAT and XRT data by the absorbed CPL model plus the blackbody function. Errors are for 90% confidence.

2.2. *Implications for the Nature of the Prompt Nonthermal Emission*

2.2.1. *Overall Spectral Properties*

We find that the prompt nonthermal emission of this event has spectral properties similar to those of the prompt γ-ray emissions

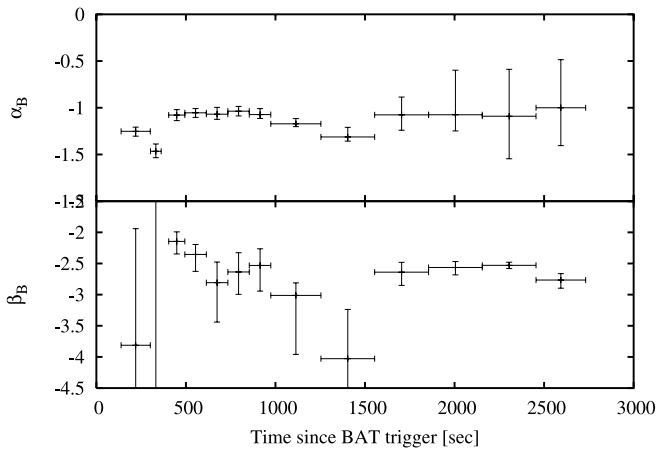

Fig. 1.—Low-energy photon index α_B and high-energy photon index β_B of the prompt nonthermal emission of GRB 060218 as functions of time, from the joint fit of the BAT and XRT data by the absorbed Band function plus the blackbody function.

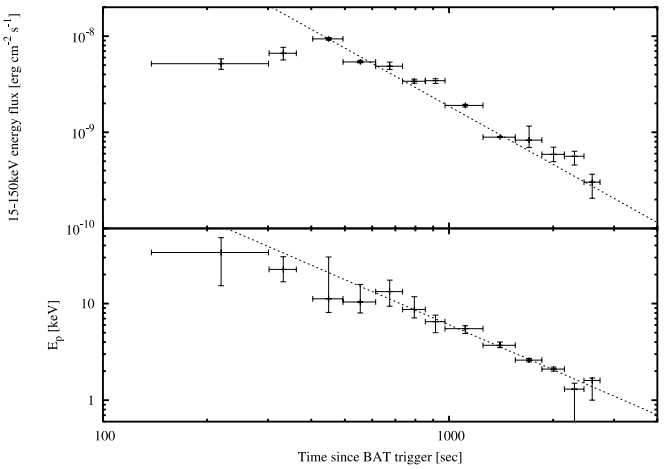

FIG. 2.—Light curve in 15–150 keV band and temporal variation of the spectral peak energy of the prompt nonthermal emission of GRB 060218, from the joint fit of the BAT and XRT data by the absorbed Band function plus the blackbody function. The dotted lines show the best-fit power-law decays, excluding the first two time bins $F(t) \propto t^{-2.0}$ and $E_p(t) \propto t^{-1.6}$.

of GRBs detected so far. The low- and high-energy photon indices α_B and β_B do not deviate significantly from $\simeq -1.0$ and $\simeq -2.5$, respectively (Fig. 1). These values are quite typical for the prompt emissions of GRBs (Preece et al. 2000). Thus, the prompt nonthermal emission may be categorized into X-ray flashes (XRFs), which are the transient events with properties similar to GRBs, except with lower spectral peak energies and smaller fluences (e.g., Sakamoto et al. 2005). The averaged spectral peak energy $\simeq 4.9$ keV and the isotropic-equivalent energy $E_{\gamma,\mathrm{iso}} \simeq 6 \times 10^{49}$ erg of the nonthermal emission obey the well-known Amati correlation, which is satisfied by the GRBs and XRFs with known redshifts, except for outliers such as GRB 980425 and GRB 031203 (Amati et al. 2002, 2006). Moreover, it has been reported that this event obeys the lag-luminosity correlation (Liang et al. 2006c; Gehrels et al. 2006).

We can confirm that the speed of the emitting region was close to the light speed. For the emission radius r_0, the condition of the transparency for the Compton scattering off the electrons associated with baryons is given in the nonrelativistic formulation by

$$\tau \simeq \frac{\sigma_{\mathrm{T}} E_{\mathrm{iso}}}{2\pi m_p c^2 \beta_0^2 r_0^2} < 1, \tag{1}$$

where E_{iso} is the isotropic-equivalent kinetic energy of the outflow, σ_{T} is the Thomson cross section, and m_p is the proton mass. Here we assume that the outflow is dominated by the kinetic energy, and E_{iso} is larger than the photon energy $E_{\gamma,\mathrm{iso}}$. Estimating that $r_0 \sim c\beta_0 \delta t$ and adopting the values $E_{\gamma,\mathrm{iso}} \simeq 6 \times 10^{49}$ erg and $\delta t \simeq 3000$ s, we obtain $\beta_0 > 0.9$. This corresponds to the Lorentz factor $\Gamma_0 > 2$. For the relativistic wind, the condition of the transparency is given by $\tau \simeq \sigma_{\mathrm{T}} L_{\mathrm{iso}}/(8\pi m_p c^3 \Gamma_0^3 r_0) < 1$ (Daigne & Mochkovitch 2002; Mészáros 2006), where L_{iso} is the isotropic-equivalent kinetic luminosity of the wind. Estimating that $L_{\mathrm{iso}} > E_{\gamma,\mathrm{iso}}/\delta t$ and $r_0 \sim \Gamma_0^2 c \delta t$, we obtain no limit on the Lorentz factor (since the maximum photon energy detected is lower than the electron's rest energy $m_e c^2$, there is no limit on the Lorentz factor from the photon annihilation or from the Compton scattering off pair-produced electrons and positrons [Kaneko et al. 2006; Lithwick & Sari 2001]). Therefore, the expansion speed of the outflow should be close to the light speed, although it is not necessarily ultrarelativistic.

All of these facts show that the prompt nonthermal emission of this event is a typical GRB (or XRF), except that its luminosity is extremely low and it is accompanied by the soft X-ray thermal component. This is one of our motivations for considering the possibility that GRB 060218 arises from a jet like typical GRBs, which we do in §§ 3 and 4. In the rest of this section, we focus on the decay phase of the prompt nonthermal emission to suggest that its emission process does not stop abruptly, but decays slowly to connect to the detected anomalous X-ray afterglow.

2.2.2. *The Decay Phase*

The decay phase of the prompt nonthermal emission is well described by $F(t) \propto t^{-2.0}$ and $E_p(t) \propto t^{-1.6}$, which implies a hardness-intensity correlation $F \propto E_p^{1.3}$. Such a correlation, $F \propto E_p^{\zeta}$, can be seen in the decay phases of the GRB prompt emissions observed by BATSE, which has a broad distribution of the power-law indices ζ, with $0.6 \lesssim \zeta \lesssim 3$ (Borgonovo & Ryde 2001; Ryde & Petrosian 2002). The *Swift* satellite has succeeded in observing the decay phases of many GRB prompt emissions more deeply than the observations in the pre-*Swift* era. The result is that the distribution of the temporal indices of the flux is also broad: $-5 \lesssim \alpha \lesssim -1$, where $F \propto t^{\alpha}$ (O'Brien et al. 2006). Thus, the flux decay of the prompt nonthermal emission of GRB 060218 is relatively shallow.

First, we argue that the decay phase is not attributable to the kinematical effect due to the curvature of the emitted region which ceased the emission process suddenly. Since the emitting shell should have a curvature, the observer receives the radiation far from the line of sight, after the cessation of the emission process. The region at a higher latitude from the line of sight has a lower velocity toward the observer, so that the emission becomes progressively dimmer and softer because of the relativistic beaming effect. This so-called curvature effect has been widely studied for the decay phases of GRB prompt emissions (Fenimore et al. 1996; Sari & Piran 1997; Kumar & Panaitescu 2000; Ryde & Petrosian 2002; Dermer 2004). *Swift* observations have suggested that the decay phases of GRB prompt emissions with temporal indices $\alpha < -2$ are due to the curvature effect (Liang et al. 2006d; Zhang et al. 2006; Lazzati & Begelman 2006; Yamazaki et al. 2006; Kobayashi & Zhang 2006).

Suppose that the shell moving with a bulk Lorentz factor Γ_0 ceases the emission at a radius r_0 and at a time t_0 and that the line of sight is within the shell, i.e., the observer views the shell on-axis. The comoving frequency ν' is boosted to $\nu = \nu' \mathcal{D}$ in the observer's frame, where $\mathcal{D} = [\Gamma_0(1 - \beta_0 \cos\theta)]^{-1}$ is the Doppler factor. Because the observed time is given by $t = t_0 - r_0 \cos\theta/c$, the Doppler factor is related to the observed time by

$$\mathcal{D} = \frac{r_0}{c\beta_0\Gamma_0}(t - t_r)^{-1}, \tag{2}$$

where $t_r \equiv t_0 - r_0/(c\beta_0)$ is the departure time of the shell from the central engine. Thus, the time-resolved spectral peak energy evolves as

$$E_p \propto \mathcal{D} \propto (t - t_r)^{-1}. \tag{3}$$

The received flux in a given time interval dt is $F_\nu\, dt \propto j'_{\nu'} \mathcal{D}^2\, d\Omega$, where $j'_{\nu'}$ is the comoving surface brightness, and the solid angle of the emitting region is related to the observed time interval by $d\Omega = 2\pi\, d(\cos\theta) \propto dt$ (Rybicki & Lightman 1979; Granot et al.

1999; Ioka & Nakamura 2001). Thus the received flux is estimated by

$$F_\nu \propto j'_{\nu'}\mathcal{D}^2 \propto (\nu')^{1+\beta_B}\mathcal{D}^2 \propto \nu^{1+\beta_B}\mathcal{D}^{1-\beta_B} \propto \nu^{1+\beta_B}(t-t_r)^{1+\beta_B}, \quad (4)$$

where we assume the high-energy Band spectrum $j'_{\nu'} \propto \nu'^{1+\beta_B}$ because the 15–150 keV band is above the peak energy E_p. With the observed value $\beta_B \simeq -2.5$, we have $F(t) \propto (t-t_r)^{-3.5}$ and $E_p(t) \propto (t-t_r)^{-1}$. To reproduce the temporal index obtained from our analysis, $t_r < 0$ is required for $F(t)$, while in contrast, $t_r > 0$ is required for $E_p(t)$. Therefore $F(t)$ and $E_p(t)$ cannot be fitted simultaneously by this model. One can also consider the structured jet model in which the spectrum and brightness vary in the angular direction (Rossi et al. 2002; Zhang & Mészáros 2002; Yamazaki et al. 2006; Dyks et al. 2006). However, the shallower flux decay requires a jet with a brighter rim, which seems implausible.

Thus the emission process is attributable not to the curvature effect of the shell which ceases the emission abruptly, but to slowly decaying emission processes. The first possibility for the decaying emission is the synchrotron emission from the external shock (Rees & Mészáros 1992; Sari et al. 1998). Since the high-energy range of the spectrum will be above the cooling frequency, the high-energy photon index $\beta_B \simeq -2.5$ corresponds to the energy distribution index of the accelerated electrons, $p \simeq 3$. The flux should then decay as $F(t) \propto t^{1/2-(3/4)p} \sim t^{-1.75}$. The characteristic frequency ν_m evolves as $t^{-3/2}$. These temporal behaviors are not inconsistent with the results of our analysis. However, the standard model gives a much lower characteristic frequency ν_m than the observed one of $\sim 10^{18}$ Hz at the deceleration time $t \simeq 500$ s with the X-ray luminosity $L_X \sim 10^{47}$ erg s^{-1}. Therefore this model is not so appealing.

The second possibility is that the decaying emission is attributed to the central engine activity. The decaying flux in the 15–150 keV range, if extrapolated as $F(t) \propto t^{-2.0}$, becomes $\sim 10^{-11}$ erg s^{-1} at $t \sim 10^4$ s. This flux is comparable to that of the detected anomalous X-ray afterglow in the 0.3–10 keV range, decaying as $F_X \propto t^{-1.1}$ with the photon index $\beta_X \simeq -3.2$, which cannot be explained within the external shock synchrotron model (Campana et al. 2006; Soderberg et al. 2006). If the anomalous X-ray afterglow is a continuation of the prompt nonthermal emission (i.e., the X-ray emission detected at $t \gtrsim 10^4$ s is not an afterglow, but the decaying prompt emission), the prompt nonthermal emission of this burst is very long (>10^6 s), and it is necessary that the photon index vary from $\beta_B \simeq -2.5$ to $\beta_X \simeq -3.2$. Ghisellini et al. (2007) have also suggested such a scenario and shown that a synchrotron inverse-Compton model could reproduce the UV/optical thermal component, as well as the prompt nonthermal emission and the anomalous X-ray afterglow. Here we note that the flux decays more steeply than t^{-1} after the peak time $t \simeq 500$ s, so the time-integrated radiation energy does not increase so much after the peak time. Thus, the total radiation energy of the prompt nonthermal emission remains $E_{\gamma,\mathrm{iso}} \simeq 6 \times 10^{49}$ erg.

The engine of this event could therefore be active for at least 10^6 s. Recent detailed observations of GRB X-ray afterglows have revealed that a number of bursts show erratic X-ray flares, which may be linked to the restartings of the central engine after the prompt emission phase (e.g., Zhang et al. 2006; Burrows et al. 2005a; Ioka et al. 2005). Since some X-ray flares are discovered $\sim 10^5$ s after the trigger, the engines of typical GRBs could also be active for $\gtrsim 10^5$ s. However, they are spiky and intermittent activities, while this event shows the smooth, power-law activity. We speculate that this indicates that the engine of this event is different from those of typical GRBs, which are believed to be black holes. Although this is just a speculation, it agrees with the analysis of the SN component of this event, which suggests that the progenitor star was less massive and collapsed to a neutron star instead of a black hole (Mazzali et al. 2006). Further discussion will be presented in § 5.

3. A JET MODEL OF THE RADIO AFTERGLOW

The afterglow of this burst shows chromatic light curves. The UV/optical afterglow is quite dim and dominated by the thermal component and the SN component (Campana et al. 2006; Ghisellini et al. 2007). The X-ray afterglow has a spectrum much steeper than those of typical GRB X-ray afterglows (Soderberg et al. 2006; Butler 2006), and it could be a continuation of the prompt nonthermal emission (see § 2.2.2). Only the radio afterglow seems rather typical and can be explained by the standard external shock synchrotron model (Soderberg et al. 2006; Fan et al. 2006). In this section, we show that the available radio data may arise from an initially collimated outflow. In the spherical outflow model, it seems difficult for a SN shock to provide the relativistic spherical ejecta with sufficient energy, as stated in § 1. In the jet model, taking into account the UV/optical and X-ray afterglows, we constrain the initial opening angle and Lorentz factor of the jet as $\theta_0 \simeq 0.3$ and $\Gamma_0 \simeq 5$, respectively. We also show that the off-axis scenario in the jet model is less likely because it requires higher γ-ray efficiency than the on-axis scenario.

3.1. *The Radio Afterglow*

For 2–22 days, the afterglow flux at 8.46 GHz is well detected and shows the power-law decay as $t^{-0.85}$. The spectrum at $t \simeq 5$ days has a peak between 1.43 and 4.86 GHz, and this peak can be interpreted as the self-absorption frequency ν_a in the standard model. This peak would not be the typical synchrotron frequency ν_m because of the small 1.43 GHz flux. Thus, the 8.46 GHz flux is most likely in the frequency range $\nu_m < \nu_a < \nu < \nu_c$, where ν_c is the cooling frequency.

In the standard model, the temporal index of the flux at each frequency range can be calculated for several cases: for a relativistic/nonrelativistic blast wave expanding into the circumburst medium of constant/wind-profile density, or for a sideways expanding relativistic blast wave. The temporal index of the flux at the frequency range $\nu_m < \nu_a < \nu < \nu_c$ for each case is $-(3/4)p + 3/4$ (relativistic blast wave, constant density), $-(3/2)p + 21/10$ (nonrelativistic blast wave, constant density), $-(3/4)p + 1/4$ (relativistic blast wave, wind-profile density), $-(7/6)p + 5/6$ (nonrelativistic blast wave, wind-profile density), and $-p$ (sideways expanding), where p is the index of the energy distribution function of the accelerated electrons (e.g., Livio & Waxman 2000; Sari et al. 1998, 1999; Chevalier & Li 1999; Frail et al. 2000). For each case to reproduce the observed temporal index of -0.85, p is required to be $\simeq$2.1, 2.0, 1.5, 1.4, and 0.9, respectively. Values of $p \gtrsim 2$ are typical for GRB afterglows (e.g., Panaitescu & Kumar 2002; Yost et al. 2003), and for this reason, we focus on the first two possibilities (i.e., the constant density cases). Note, however, that the possibilities for $p < 2$ (i.e., the wind-profile density cases and the sideways expanding case) cannot be ruled out.

For the two possibilities of the standard model, the available radio data requires the following three conditions.

1. The spectrum peaks at $\nu_a \sim 4 \times 10^9$ Hz at $t \simeq 5$ days.
2. The flux at 22.5 GHz is $\sim$0.25 mJy at $t \simeq 3$ days.

3. The cooling frequency is $\nu_c \leq 5 \times 10^{15}$ Hz, so that the synchrotron spectrum of the external shock electrons does not dominate the detected anomalous X-ray afterglow.

3.1.1. *Relativistic Blast Wave Model*

Fan et al. (2006) have modeled the first possibility, i.e., the synchrotron spectrum from the relativistic blast wave with $p \simeq 2.1$ expanding into the constant density medium, and derived three constraints on the physical parameters of the afterglow from the above three conditions (1)–(3) (their equations [8]–[10]). The satisfying parameters they have suggested are the isotropic-equivalent kinetic energy of the outflow $E_{k,\rm iso} \sim 10^{50}$ erg, the number density of the circumburst medium $n \sim 10^2$ cm^{-3}, and the ratios of the accelerated electron energy and the magnetic energy to the shocked thermal energy $\epsilon_e \sim 10^{-2}$ and $\epsilon_B \sim 10^{-3}$, respectively. With these parameters, the Lorentz factor of the outflow is estimated as $\Gamma \approx 2(t/1\ \rm day)^{-3/8}$. If the opening angle of the outflow is $\theta_0 \leq 1$, the outflow will begin to expand sideways at $t \leq 6$ days, and the radio light curves will break (Rhoads 1999). However, the actual light curve does not show such a break, so it is concluded that $\theta_0 > 1$ in this model, i.e., the outflow is spherical. In this case, the outflow becomes nonrelativistic at $t \simeq 6$ days, and the radio flux varies from $t^{-0.85}$ to $t^{-1.1}$. This is consistent with the available radio light curves (Fan et al. 2006).

The parameters $E_{k,\rm iso} \sim 10^{48}$ erg, $n \sim 10^2$ cm^{-3}, $\epsilon_e \sim 10^{-1}$, and $\epsilon_B \sim 10^{-1}$ also satisfy the above three constraints and fit the radio data (Soderberg et al. 2006). However, since the isotropic-equivalent γ-ray energy is $E_{\gamma,\rm iso} \simeq 6 \times 10^{49}$ erg, the inferred γ-ray efficiency is extremely high; $\eta_\gamma \equiv E_{\gamma,\rm iso}/(E_{\gamma,\rm iso} + E_{k,\rm iso}) \sim 98\%$, and thus this parameter set is implausible.

The relativistic spherical outflow is not consistent with the standard collapsar scenario, in which a relativistic collimated outflow digs a narrow hole in the progenitor star without loading so much stellar matter (Woosley 1993; MacFadyen & Woosley 1999). Thus, one may consider a scenario in which a spherical outflow is accelerated to a mildly relativistic speed as the SN shock sweeps the stellar envelope with a steep density gradient (Matzner & McKee 1999; Tan et al. 2001). However, it seems impossible that the required kinetic energy $E_{k,\rm iso} \sim 10^{50}$ erg is transferred into the relativistic ejecta by the SN with the total kinetic energy $\simeq 10^{51}$ erg (Mazzali et al. 2006), as discussed in § 1. For this reason, we conclude that the first possibility is quite unlikely.

3.1.2. *Nonrelativistic Blast Wave Model*

We now investigate the second possibility: that the radio afterglow may arise from the nonrelativistic phase of an initially jetted outflow with $p \simeq 2.0$ expanding into the constant density medium. The relativistic jet is decelerated and subsequently expands sideways, finally becoming nonrelativistic at a certain transition time t_s. The transition time is estimated by requiring that the speed of the Sedov-Taylor blast wave be close to the light speed, i.e., $\beta = (2/5c)[E_k/(nm_p t^3)]^{1/5} \sim 1$, where E_k is the kinetic energy of the spherical blast wave (see Livio & Waxman 2000):

$$t_s \simeq 7.5 \times 10^6\ \rm s \left(\frac{E_{k,51}}{n}\right)^{1/3}. \quad (5)$$

Here (and hereafter) we have adopted the notation $Q = 10^x Q_x$ in cgs units. Since the available 8.46 GHz light curve does not show the sideways expanding relativistic phase $t^{-p} \sim t^{-2}$, we require $t_s \lesssim 2$ days.

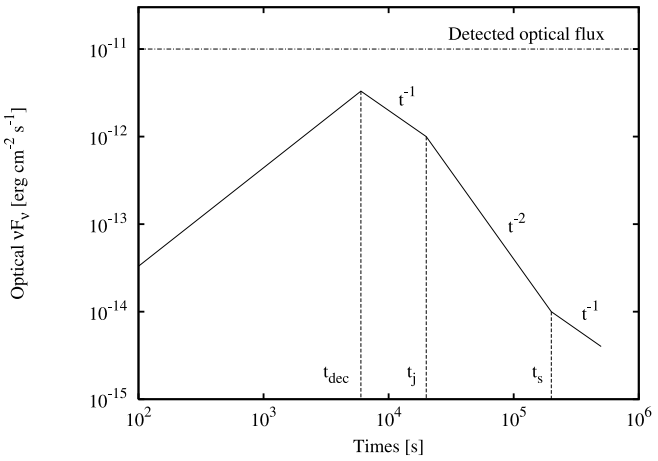

FIG. 3.—Schematic picture of the optical νF_ν flux from the external shock in our jet model (*solid line*), which does not exceed the detected optical flux shown in Ghisellini et al. (2007) and Campana et al. (2006) (*dot-dashed line*). The outflow in our jet model is decelerated at $t_{\rm dec}$ followed by the Blandford-McKee evolution $F_{\rm opt} \propto t^{-1}$, begins to expand sideways at t_j followed by the evolution $F_{\rm opt} \propto t^{-2}$, and finally shifts at t_s into the Sedov-Tailor evolution $F_{\rm opt} \propto t^{-1}$.

Three constraints on the physical parameters of the afterglow are given by conditions (1)–(3) in the first part of this subsection (§ 3.1). Assuming that the minimum Lorentz factor of the accelerated electrons is $\gamma_m \simeq 10^{-1}\beta^2 \epsilon_e m_p/m_e$, we may derive the following three constraints on the physical parameters:

$$\epsilon_{e,-1}^{1/3} \epsilon_{B,-2}^{1/3} E_{k,51}^{1/3} n^{1/3} \sim 1, \quad (6)$$

$$\epsilon_{e,-1} \epsilon_{B,-2}^{0.75} E_{k,51}^{1.3} n^{0.45} \sim 3 \times 10^{-3}, \quad (7)$$

$$\epsilon_{B,-2}^{1.5} E_{k,51}^{0.6} n^{0.9} \geq 0.4. \quad (8)$$

The results are similar to those derived in the relativistic blast wave model (see § 3.1.1 and Fan et al. 2006). These constraints and the requirement of $t_s \lesssim 2 \times 10^5$ s are satisfied by $E_k \simeq 2 \times 10^{48}$ erg, $n \simeq 10^2$ cm^{-3}, $\epsilon_e \simeq 10^{-1}$, and $\epsilon_B \simeq 10^{-1}$.

Then the isotropic-equivalent kinetic energy before sideways expansion is estimated by $E_{k,\rm iso} = 2E_k/\theta_0^2 \simeq 4 \times 10^{48} \theta_0^{-2}$ erg. To obtain a reasonable γ-ray efficiency, $\eta_\gamma = E_{\gamma,\rm iso}/(E_{\gamma,\rm iso} + E_{k,\rm iso}) \lesssim 0.5$ (Lloyd-Ronning & Zhang 2004; Ioka et al. 2006; Fan & Piran 2006; Granot et al. 2006; Zhang et al. 2007), the opening angle $\theta_0 \lesssim 0.3$ is favorable. In the following section, we further constrain the opening angle and also the Lorentz factor of the jet, using the observed UV/optical and X-ray emission.

3.2. *Constraints from the UV/Optical and X-ray Afterglow*

In our model ($E_k \simeq 2 \times 10^{48}$ erg, $n \simeq 10^2$ cm^{-3}, $\epsilon_e \simeq 10^{-1}$, and $\epsilon_B \simeq 10^{-1}$), the characteristic parameters at $t \simeq 5$ days are calculated as $F_{\nu,\rm max} \sim 2 \times 10^{-25}$ erg cm^{-2} s^{-1} Hz^{-1}, $\nu_m \simeq 5 \times 10^6$ Hz, $\nu_a \simeq 4 \times 10^9$ Hz, and $\nu_c \simeq 7 \times 10^{13}$ Hz. Thus the optical νF_ν flux at this time is $\sim 10^{15} F_{\nu,\rm max} (\nu_c/\nu_m)^{-0.5} (10^{15}/\nu_c)^{-1} \simeq 4 \times 10^{-15}$ erg cm^{-2} s^{-1}. If we trace back to earlier times through the standard jet model, the optical flux gets much higher than this value (see Fig. 3). The detected optical flux at 10^4–10^5 s is dominated by the thermal component with $\nu F_\nu \sim 10^{-11}$ erg cm^{-2} s^{-1} (Ghisellini et al. 2007; Campana et al. 2006). The requirement that the synchrotron flux from our jet not exceed this flux gives constraints on the initial opening angle θ_0 and the initial Lorentz factor Γ_0 of the jet.

The external shock of the jet progressively experiences the Blandford-McKee evolution, the sideways expanding evolution, and the Sedov-Taylor evolution. For each evolution phase, the

characteristic frequencies of the synchrotron spectrum with $p \simeq 2.0$ vary as $\nu_m \propto t^{-1.5}$, t^{-2}, and t^{-3}; $\nu_a(>\nu_m) \propto t^{-2/3}$, $t^{-0.5}$, and $t^{-2/3}$; $\nu_a(<\nu_m) \propto t^{0}$, $t^{-0.2}$, and $t^{1.2}$; and $\nu_c \propto t^{-0.5}$, t^{0}, and $t^{-0.2}$ (e.g., Sari et al. 1998, 1999; Livio & Waxman 2000). If we trace back to $t \sim 10^4$ s, ν_m, ν_a, and ν_c all remain lower than the optical band. Thus for $t \gtrsim 10^4$ s, the optical band is at the range $\nu > \nu_c$, and the optical energy flux evolves as t^{-1} at the Blandford-McKee phase, t^{-2} at the sideways expanding phase, and t^{-1} at the Sedov-Taylor phase. With these behaviors of the optical flux from the external shock, we suggest the following possible jet scenario (see Fig. 3 for a schematic picture of the optical light curve). The external shock of the jet is decelerated at $t_{\rm dec} \simeq 6 \times 10^3$ s, begins to expand sideways at $t_j \simeq 2 \times 10^4$ s, and shifts to the Sedov-Taylor expansion at $t_s \simeq 2 \times 10^5$ s. The peak optical flux is $\nu F_\nu \simeq 3 \times 10^{-12}$, which is less than the observed one, so the optical afterglow estimated within our jet model is not inconsistent with the available optical data.

Since the X-ray band is also above ν_c and $p \simeq 2.0$, the X-ray νF_ν flux is comparable to the optical one. Thus, this external shock emission does not overwhelm the observed anomalous X-ray afterglow shown in Campana et al. (2006) and Soderberg et al. (2006).

We now give reasonable values of θ_0 and Γ_0. At the sideways expansion phase, the opening angle of the jet evolves as $\theta = \Gamma^{-1} \propto t^{1/2}$ (Rhoads 1999; Sari et al. 1999) and finally becomes $\theta \simeq 1$ at the transition time t_s to the Sedov-Taylor expansion phase. The initial opening angle of the jet is thus determined by

$$\theta_0 \left(\frac{t_s}{t_j} \right)^{1/2} \simeq 1. \tag{9}$$

When $t_s \simeq 2 \times 10^5$ s and $t_j \simeq 2 \times 10^4$ s are adopted, we obtain $\theta_0 \simeq 0.3$. If θ_0 is smaller, the ratio t_s/t_j is larger. At the Blandford-McKee phase, the Lorentz factor of the jet evolves as $\Gamma \propto t^{-3/8}$ and finally becomes $\Gamma \simeq \theta_0^{-1}$ at the jet-break time t_j. The initial Lorentz factor of the jet is thus determined by

$$\Gamma_0 \left(\frac{t_j}{t_{\rm dec}} \right)^{-3/8} \simeq \theta_0^{-1}. \tag{10}$$

When $t_j \simeq 2 \times 10^4$ s and $t_{\rm dec} \simeq 6 \times 10^3$ s are adopted, we obtain $\Gamma_0 \simeq 5$. If Γ_0 is larger, the ratio $t_j/t_{\rm dec}$ is larger. The upper bound of the optical data does not allow values of t_s/t_j and $t_j/t_{\rm dec}$ larger than those we have adopted, and therefore it does not allow the smaller θ_0 and the larger Γ_0. Since the consideration about the γ-ray efficiency requires $\theta_0 \lesssim 0.3$ (see § 3.1.2), the opening angle is restricted to a narrow range around $\theta_0 \simeq 0.3$.

In summary, we have obtained a jet model for the radio afterglow of GRB 060218, with $\theta_0 \simeq 0.3$, $\Gamma_0 \simeq 5$, $E_{k,\rm iso} \simeq 4 \times 10^{49}$ erg, and $\eta_\gamma \simeq 0.6$, which is compatible with the UV/optical and X-ray data. The collimation-corrected energy of the jet is $E_j \simeq (E_{\gamma,\rm iso} + E_{k,\rm iso})\theta_0^2/4 \simeq 10^{48}$ erg. Assuming that the duration of the prompt nonthermal emission $\delta t \sim 10^3$ s is the active time of the central engine δT, the luminosity of the jet is estimated by $L_j \sim E_j/\delta T \sim 10^{45}$ erg s^{-1}.

3.3. *Off-Axis Scenario*

In the above arguments in §§ 2 and 3, we have assumed that the observer views the jet from the on-axis direction and the luminosity of the prompt nonthermal emission is intrinsically low. It is possible that the low luminosity of GRB 060218 can be attributed to a typical bright GRB jet viewed off-axis (e.g., Yamazaki et al. 2003; Ramirez-Ruiz et al. 2005; Granot et al. 2005; Toma et al. 2005). However, we find that the off-axis scenario is less likely than the on-axis scenario, since a higher γ-ray efficiency is required.

Since the outflow is spherical when the radio afterglow is observed, the off-axis scenario is the same as the on-axis one in this phase. Thus, the isotropic-equivalent kinetic energy is determined by $E_{k,\rm iso} = 2E_k/\theta_0^2 \simeq 4 \times 10^{48} \theta_0^{-2}$ erg. In the off-axis scenario, the isotropic-equivalent γ-ray energy $E_{\gamma,\rm iso,on}$ measured from an on-axis viewpoint is larger than the observed one $E_{\gamma,\rm iso} \simeq 6 \times 10^{49}$ erg. So the γ-ray efficiency is expected to be higher than that estimated within the on-axis scenario (e.g., Toma et al. 2006).

To obtain the smaller γ-ray efficiency, we could consider $\theta_0 < 0.3$. However, a smaller θ_0 leads to an even higher γ-ray efficiency, as we see below. The smaller θ_0 requires $t_j < 10^4$ s, and then the optical flux, if received from the on-axis direction, exceeds the constraint from the detected optical afterglow (see Fig. 3). To escape the constraint, the synchrotron flux from the off-axis jet should peak at some time t_v after t_j. The peak occurs when the line of sight enters the relativistic beaming cone of the emission from the edge of the sideways expanding jet, i.e., $\theta_v \sim \theta + \Gamma^{-1} \simeq 2\Gamma^{-1}$. The Lorentz factor varies as $\Gamma \propto t^{-1/2}$ in the sideways expansion phase and becomes $\Gamma \sim 1$ at t_s, and thus the following equation is satisfied:

$$\frac{1}{2}\theta_v \left(\frac{t_s}{t_v} \right)^{1/2} \simeq 1. \tag{11}$$

Since t_v should be greater than 10^4 s, we obtain $\theta_v \gtrsim 0.4$. The isotropic-equivalent γ-ray energy measured from an on-axis viewpoint is roughly estimated by $E_{\gamma,\rm iso,on} \approx [\Gamma_0(\theta_v - \theta_0)]^6 E_{\gamma,\rm iso} > 10^{47}\Gamma_0^6$ erg, where we have used $\theta_v > \theta_0$. With $\Gamma_0 \geq \theta_0^{-1}$, we obtain $E_{\gamma,\rm iso,on} > 10^{47}\theta_0^{-6}$ erg. For $\theta_0 < 0.3$, this leads to a higher γ-ray efficiency than the on-axis scenario: $\eta_\gamma > 0.7$. We may therefore conclude that the off-axis scenario is unlikely for this event.

4. A COLLAPSAR MODEL OF GRB 060218

In the previous section, we have obtained a possible jet model that is consistent with the available afterglow data. Our jet model requires an opening angle $\theta_0 \simeq 0.3$, which is somewhat larger than those of typical cosmological GRBs (e.g., see Ghirlanda et al. 2004), and an extremely small luminosity $L_j \sim 10^{45}$ erg s^{-1}, which is about 10^5 times smaller than those of typical cosmological GRBs. One may then wonder whether such a wide and low-luminosity jet can penetrate a progenitor star. It is possible for a jet to become nonrelativistic if it loads so much stellar matter with a large cross section. Matzner (2003) has discussed analytically several conditions for making a hole in the collapsar model. We extend his theoretical considerations to conclude that an adiabatic cold jet is excluded, but a nonadiabatic hot jet is appropriate for this event. (Our argument can be also applied to typical GRB jets, and some wide GRB jets also would need to be hot.)

4.1. *The Motion of a Jet Head*

The standard collapsar model assumes that a black hole or a neutron star with an accretion disk is formed after an iron core of the massive progenitor star collapses and that the system produces a jet (Woosley 1993; MacFadyen & Woosley 1999). Since the free-fall timescale of a stellar envelope is longer than, or comparable with, the crossing timescale for the jet to propagate within the progenitor star and to hit its surface, the stellar envelope would disturb the progress of the jet.

Consider the progress of a relativistic jet outward through the stellar envelope. Two shocks form: a reverse shock reducing the jet speed and increasing its internal energy and a forward shock that propagates into the surrounding stellar envelope, giving it internal energy. As a result, there are four distinct regions in this system: the propagating jet, the head of the jet lying between the two shocks, the stellar envelope, and a cocoon consisting of shocked jet and shocked ambient material (see Fig. 2 of Matzner 2003). This system is similar to classical double radio sources (Begelman & Cioffi 1989).

Two conditions are required for a jet to break out of the star relativistically. First, the Lorentz factor of the jet head Γ_h should be smaller than the inverse of the opening angle of the jet, θ. If so, the shocked material may escape sideways to form the cocoon, and the jet may avoid baryon loading. Second, the speed of the jet head should be larger than that of the expanding cocoon,

$$\beta_h > \beta_c. \tag{12}$$

If this condition is violated, the cocoon expands spherically around the jet and finally explodes the star, producing a nonrelativistic dense spherical outflow. When the above two conditions are satisfied, we may consider the longitudinal balance of the momentum flux in the frame of the jet head,

$$w_j \Gamma_j^2 \Gamma_h^2 (\beta_j - \beta_h)^2 + p_j = w_a \Gamma_h^2 \beta_h^2 + p_a. \tag{13}$$

Here the subscripts j and h describe the jet and the jet head, respectively, and w ($\equiv e + p$), p, and e are the enthalpy, the pressure, and the energy density including rest energy density ρc^2, respectively. For stellar envelopes, $p_a \ll \rho_a c^2$ and $w_a = \rho_a c^2$ are good approximations.

If Γ_j is significantly larger than unity, p_j can be neglected in the left-hand side of equation (13), and we obtain $(\beta_h^{-1} - 1)^{-2} = w_j \Gamma_j^2 / (\rho_a c^2) = L_{\rm iso}/(4\pi r^2 \rho_a c^3)$, where in the last equality we introduce the isotropic-equivalent luminosity $L_{\rm iso}$ of the jet. For the jet to drive the explosion of the star, this equation should be satisfied when $r = R$, where R is the radius of the progenitor star, so that $(\beta_h^{-1} - 1)^{-2} \approx 10^{-3} L_{\rm iso,51} (R/R_\odot)^{-2} \rho_a^{-1}$. This factor is much less than unity for the parameters of typical GRBs (and so for the low-luminosity GRBs), so the jet head is found to be nonrelativistic. Thus, with the collimation-corrected luminosity of the jet $L_j = w_j \Gamma_j^2 c \pi r^2 \theta^2$, we obtain

$$\beta_h \approx \left(\frac{L_j}{\pi r^2 \theta^2 \rho_a c^3} \right)^{1/2}. \tag{14}$$

We take $\rho_a \sim M/(4\pi R^3/3)$ for simplicity, where M is the total mass of the progenitor star.

4.2. *Cocoon Structure*

The cocoon drives a shock into the stellar envelope, which expands nonrelativistically at the velocity β_c given by the transverse balance of the cocoon pressure and the ram pressure of the stellar envelope,

$$p_c = \rho_a c^2 \beta_c^2. \tag{15}$$

The pressure of the cocoon p_c is roughly constant away from the jet head and is approximated by $E_{\rm in}/(3V_c)$, with the thermal energy $E_{\rm in}$ deposited in the cocoon with volume V_c. Since the jet head is nonrelativistic, most of the kinetic energy of the jet gets thermalized through the reverse shock. The cocoon energy is the energy caught by the jet head, which is calculated by $E_{\rm in} = \int_0^r (L_j\, dr/c\beta_h) \simeq L_j (r/c\beta_h)$. The cocoon length is given by $r \simeq c\beta_h t$, as long as $\beta_h > \beta_c$ is satisfied, and the cocoon width is given by $R_c \simeq c\beta_c t$. So the cocoon volume is roughly $V_c \simeq (\pi/3) R_c^2 r \simeq (\pi/3) r^3 \beta_c^2/\beta_h^2$. The cocoon pressure can therefore be written as $p_c \simeq L_j \beta_h / (\pi r^2 c \beta_c^2)$. Equation (15) gives us the following equations:

$$\beta_c = \left(\frac{L_j}{\pi r^2 \rho_a c^3} \beta_h \right)^{1/4}, \tag{16}$$

$$p_c = \left(\frac{L_j}{\pi r^2} \rho_a c \beta_h \right)^{1/2}, \tag{17}$$

which describe the velocity and the pressure of the cocoon with the parameters of the jet and the stellar envelope within the assumption of $\beta_h > \beta_c$.

4.3. *Cold Jet*

Here we examine an adiabatic jet that propagates ballistically in the progenitor star (see also Mészáros & Rees 2001; Waxman & Mészáros 2003). An important point is that the opening angle and the Lorentz factor of the cold ballistic jet do not change after exiting the progenitor star. If the opening angle and Lorentz factor of the jet at the breakout are $\theta_{\rm br}$ and $\Gamma_{\rm br}$, they are also $\theta_0 = \theta_{\rm br}$ and $\Gamma_0 = \Gamma_{\rm br}$ after exiting the star. In contrast, a hot jet which propagates nonadiabatically by the interaction between the jet and the cocoon and stays dominated by the internal energy, changes its opening angle and Lorentz factor through the free expansion outside the star. The hot jet is discussed in the next subsection.

For the jet to drive an explosion, the consistency $\beta_h > \beta_c$ should be satisfied. From equations (14) and (16), this leads to the constraint on the opening angle of the jet,

$$\theta < \left(\frac{L_j}{\pi r^2 \rho_a c^3} \right)^{1/6}. \tag{18}$$

For GRB 060218, the underlying SN is Type Ic, which implies that the progenitor star is a C/O Wolf-Rayet star (e.g., Mazzali et al. 2006). Its radius and mass are typically $R \sim 10^{11}$ cm and $M \sim 10^{34}$ g, respectively. The averaged mass density ρ_a is then $\sim$1 g cm^{-3}. For the luminosity $L_j \sim 10^{45}$ erg s^{-1}, the opening angle of the jet at the breakout (i.e., when $r = R$) is constrained to $\theta_{\rm br} < 0.03$, so that $\theta_0 < 0.03$ within the cold jet scenario. The value of the opening angle suggested in our jet model ($\theta_0 \simeq 0.3$) violates this constraint. The cold jet scenario is therefore excluded for this event.

A wide cold jet may be allowed if the jet is being launched long after the cocoon explodes the star, since the ambient density ρ_a drops through the expansion in equation (18). However, the star must expand from $R_c \sim 10^{11}$ to $\sim 10^{17}$ cm in order to allow $\theta_0 \simeq 0.3$, which is unlikely.

4.4. *Hot Jet*

Next we consider the possibility that the jet is dominated by the internal energy throughout the propagation in the progenitor star (see also Lazzati & Begelman 2005). At the jet-cocoon boundary, oblique shocks and shear instabilities may occur and dissipate the kinetic energy of the jet. This situation can be seen in several numerical simulations of the collapsar model (Aloy et al. 2000; Zhang et al. 2003, 2004; Umeda et al. 2005; Mizuta et al. 2006).

In contrast to the cold jet, the hot jet expands freely after exiting the star. As a result, the opening angle is determined by the

Lorentz factor $\Gamma_{j,\rm ex}$ just before exiting the star. In the comoving frame of the hot material moving outward relativistically with Lorentz factor $\Gamma_{j,\rm ex}$, the hot material will expand freely and finally get the Lorentz factor $\Gamma' = e/\rho_j c^2$. In the laboratory frame, the material will be beamed into the opening angle

$$\theta_0 \sim \Gamma_{j,\rm ex}^{-1}, \tag{19}$$

and the Lorentz factor of the material is given by $\Gamma_0 \sim \Gamma'\Gamma_{j,\rm ex}(1+\beta'\beta_{j,\rm ex}) \sim 2\Gamma'\Gamma_{j,\rm ex}$. Note that $\Gamma_0\theta_0 \sim 2\Gamma' > 1$ is satisfied.

For GRB 060218, $\Gamma_{j,\rm ex} \sim \theta_0^{-1} \simeq 3$ is required to reproduce $\theta_0 \simeq 0.3$. For the initial Lorentz factor of the jet exiting the star to be $\Gamma_0 \simeq 5$, $\Gamma' = e/\rho_j c^2 \sim 1$–$2$ is favorable. Therefore, the jet of this burst may originate from a mildly hot jet in which the internal energy e is comparable with the rest energy $\rho_j c^2$ before exiting the star.

4.4.1. *The Breakout Timescale*

Let us estimate the breakout timescale. We expect that the breakout timescale is not much larger than the active time of the central engine after the breakout $\delta T \sim 10^3$ s. Otherwise, the engine has to stop suddenly just after breaking out of the star, which seems unlikely.

For the hot jet, $p_j \gg \rho_j c^2$ and $w_j = 4p_j$ are good approximations, and thus $p_j = L_j/(4\Gamma_j^2 c\pi r^2\theta^2)$. Before the breakout, the opening angle of the hot jet is determined by the transverse pressure balance between the jet and the cocoon,

$$p_j = p_c. \tag{20}$$

Using equations (14) and (17), we obtain

$$\theta = \left(\frac{L_j}{256\pi r^2\rho_a c^3}\right)^{1/6}\Gamma_j^{-4/3}, \tag{21}$$

which satisfies the consistency of $\beta_h > \beta_c$ (eq. [18]). For GRB 060218, adopting the values $L_j \sim 10^{45}$ erg s^{-1}, $R \sim 10^{11}$ cm, $\rho_a \sim 1$ g cm^{-3}, and $\Gamma_j \simeq 3$, we obtain the opening angle at the breakout time as $\theta_{\rm br} \sim 3\times10^{-3}$.

The velocities of the jet head (eq. [14]) and the cocoon (eq. [16]) are calculated using eq. (21),

$$\beta_h = \left(\frac{16L_j}{\pi r^2\rho_a c^3}\right)^{1/3}\Gamma_j^{4/3}, \tag{22}$$

$$\beta_c = \left(\frac{2L_j}{\pi r^2\rho_a c^3}\right)^{1/3}\Gamma_j^{1/3}. \tag{23}$$

The ratio of the two velocities is $\beta_h/\beta_c = 2\Gamma_j$. Then, if Γ_j is close to unity, we have $\beta_c \sim \beta_h$, and hence the cocoon expands quasi-spherically. This situation is in good agreement with a recent series of numerical simulations performed by Mizuta et al. (2006). They have argued that the morphology of the explosion depends on the Lorentz factor $\Gamma_{j,0}$ of the jet given at the inner boundary: when the Lorentz factor is high ($\Gamma_{j,0} \gtrsim 3$), the high-pressure cocoon collimates the outflow to form a narrow, relativistic jet, and when the Lorentz factor is low, on the contrary, the outflow is not collimated and expands quasi-spherically.

The breakout timescale is determined by $t_{\rm br} = R/(c\beta_{h,\rm br})$, where $\beta_{h,\rm br}$ is the velocity of the jet head (eq. [22]) obtained at $r = R$:

$$t_{\rm br} \simeq \left(\frac{16L_j}{\pi\rho_a}\right)^{-1/3}R^{5/3}\Gamma_j^{-4/3}. \tag{24}$$

For GRB 060218, we obtain $t_{\rm br} \sim 300$ s, which is a reasonable value. The hot jet of this event takes $t_{\rm br} \sim 300$ s to break out of the progenitor star and lasts a further $\delta T \sim 10^3$ s to eject the material producing the prompt emission.

4.4.2. *A Possible Additional Widening Effect*

After the breakout time, the opening angle of the jet before exiting the star might become wider than the value $\theta_{\rm br} \sim 3\times10^{-3}$, which is determined by the pressure balance between the jet and the cocoon. The cocoon expands freely outward from the star after the breakout time, and finally the cocoon pressure becomes negligible in $R/(c/\sqrt{3}) \sim 10$ s. The cocoon shock that will sweep the stellar envelope is not so strong, and the envelope would remain cold. After the cocoon disappears, the jet opening angle would be determined by the transverse balance between the jet pressure and the ram pressure of the stellar envelope matter. The balance equation in the comoving frame of the propagating jet is

$$p_j = (\Gamma_j\rho_a)(r\dot{\theta})^2, \tag{25}$$

where r is the radial coordinate in the laboratory frame. The Lorentz factor appearing in the right-hand side is due to the Lorentz transformation. Substituting $p_j = L_j/(4\Gamma_j^2\pi r^2\theta^2 c)$, we find that θ gradually increases, since the jet pushes the stellar envelope. Let L_j and Γ_j be constant; integrating over time, we obtain

$$\theta = \left(\frac{L_j}{\pi\rho_a c}\right)^{1/4}r^{-1}\Gamma_j^{-3/4}\delta T^{1/2}. \tag{26}$$

For GRB 060218, if we adopt the values $L_j \sim 10^{45}$ erg s^{-1}, $\rho_a \sim 1$ g cm^{-3}, $r = R \sim 10^{11}$ cm, $\Gamma_j \simeq 3$, and $\delta T \sim 10^3$ s, we obtain $\theta \sim 0.1$. This is less than the opening angle after free expansion, $\theta_0 \simeq 0.3$, in eq. (19), so the widening effect is not important in this event. In some cases, the widening effect could dominate the free expansion effect.

5. SUMMARY AND DISCUSSION

We have investigated whether GRB 060218 arises from a collimated jet. So far, the lack of the jet break has led to the interpretation that the outflow of this event is spherical and thereby that the outflow is not the standard collapsar jet but the outermost parts of the stellar envelope that the SN shock accelerates to a mildly relativistic speed (Soderberg et al. 2006; Fan et al. 2006). However, we have shown that the available radio data may be interpreted as a nonrelativistic phase of an initially collimated outflow within the standard external shock synchrotron model, and that the jet model with an initial opening angle $\theta_0 \simeq 0.3$, Lorentz factor $\Gamma_0 \simeq 5$, and a collimation-corrected luminosity $L_j \sim 10^{45}$ erg can explain the radio data and is compatible with the UV/optical and X-ray data. This model is more natural than the initially spherical outflow model, because in the latter model, the relativistic ejecta for the prompt and afterglow emission with $\simeq 10^{50}$ erg could not be produced by the underlying SN with total kinetic energy $\simeq 10^{51}$ erg (Mazzali et al. 2006). Furthermore, the jet model is supported by the recent report of the detection of optical linear polarization in the SN component of this event (Gorosabel et al. 2006). We also show that the jet of this event can penetrate the progenitor star by extending the analytical considerations by Matzner (2003). The jet would be

relativistically hot in the progenitor star and hence expand freely outside the star into the relatively wide opening angle. The off-axis scenario within the jet model is unlikely because it requires an unrealistically high γ-ray efficiency.

With the jet opening angle $\theta_0 \simeq 0.3$, the collimation-corrected γ-ray energy of this event is $E_\gamma \simeq 3 \times 10^{48}$ erg, which makes this event consistent with the Ghirlanda correlation (Ghirlanda et al. 2004; Ghisellini et al. 2006).

For the prompt emission, we have analyzed the BAT and XRT data and found that the nonthermal component of the prompt emission may be fitted by the Band function, similar to other GRBs. The low- and high-energy photon indices are almost constant with $\alpha_B \simeq -1$ and $\beta_B \simeq -2.5$, respectively, which are quite typical features of GRBs. The 15–150 keV flux of the prompt nonthermal emission shows a relatively shallow decay, and we show that this decay is not due to the curvature effect of the emitting shell that suddenly ceases the emission process. The decay of the nonthermal emission may directly connect to the anomalous X-ray afterglow detected up to $t \simeq 10^6$ s. If this is correct, the central engine might be active for $\gtrsim 10^6$ s. In summary, the low-luminosity GRB 060218 has a typical prompt nonthermal emission and may originate from a standard collapsar jet, possibly driven by a long-acting central engine.

A number of *Swift* GRBs show late-time X-ray flares, which may be attributed to the long intermittent activities of their central engines (e.g., Zhang et al. 2006; Ioka et al. 2005). In contrast, the engine of this burst might have the long power-law activity. It is then possible that the engine of this burst is different from those of typical GRBs, which are believed to be black holes. Mazzali et al. (2006) have performed a detailed modeling of the spectra and light curve of the SN component and argued that the progenitor star of this event had a smaller mass than other GRB-SNe, suggesting that a neutron star rather than a black hole was formed as the central engine of the jet. The intrinsic rate of such low-luminosity GRBs would be larger than the local rate of typical cosmological GRBs (Soderberg et al. 2006; Pian et al. 2006; Cobb et al. 2006; Liang et al. 2006a). For these reasons, low-luminosity GRBs might be a distinct GRB population involving neutron star engines. We speculate that massive progenitor stars form black holes at the core collapse, which produce highly relativistic jets, making high-luminosity GRBs with strong spiky prompt emissions and flares, while less massive progenitor stars form neutron stars, which produce mildly relativistic jets, making low-luminosity GRBs with weak, smooth prompt emissions.

If the opening angles of the low-luminosity GRBs are around $\sim$0.3, the true rate of the low-luminosity GRBs with a beaming correction is $R_{\rm LL} \sim 10^3$ Gpc^{-3} yr^{-1}. The local rate of Type Ibc SNe is $R_{\rm SN} \sim 10^4$ Gpc^{-3} yr^{-1} (Soderberg et al. 2006; Dahlen et al. 2004; Cappellaro et al. 1999). Then the low-luminosity GRBs might be created at a rate $\sim$10% of that of Type Ibc SNe. By comparison, the collimation-corrected rate of typical cosmological GRBs is $\sim$1% of that of Type Ibc SNe. Note that it is also suggested that the birthrate of Galactic magnetars is $\sim$10% of the SN rate (Kouveliotou et al. 1998).

Now, if the neutron star loses its rotational energy mainly through magnetic dipole radiation, and a fraction of energy f is transferred to the jet, then the luminosity of the jet is approximated by (Shapiro & Teukolsky 1983)

$$L_j \sim f L_0 \left(1 + \frac{t}{\tau}\right)^{-2}, \tag{27}$$

where

$$L_0 = \frac{B^2 R_s^6 \Omega_0^4}{6c^3} \sim 10^{47}\ {\rm erg\ s^{-1}}\ B_{16}^2 R_{s,6}^6 P_{0,-2}^{-4}, \tag{28}$$

$$\tau = \frac{3c^3 I}{B^2 R_s^6 \Omega_0^2} \sim 10^3\ {\rm s}\ I_{45} B_{16}^{-2} R_{s,6}^{-6} P_{0,-2}^2. \tag{29}$$

Here B is the magnetic field strength at the pole, R_s is the neutron star radius, Ω_0 is the initial angular frequency, $P_0 = 2\pi/\Omega_0$ is the initial rotation period, and I is the moment of inertia of the neutron star. The characteristic spin-down timescale τ might be the peak time $t \sim 10^3$ s of the prompt nonthermal emission, and the temporal decay of the spin-down luminosity after τ, $L_j \propto t^{-2}$, might agree with that of the prompt nonthermal emission flux, $F \propto t^{-2.0}$, shown in Figure 2. Assuming $f \sim 10^{-2}$, we obtain $B \sim 10^{16}$ G and $P_0 \sim 10$ ms in order that $L_j \sim 10^{45}$ erg s^{-1} and $\tau \sim 10^3$ s are reproduced. In this case, the rotational energy $I\Omega^2/2$ would be overwhelmed by the magnetic energy $(B^2/8\pi)(4\pi R_s^3/3)$ at $t \sim 10^4$ s. This timescale is comparable to the transition time of the decay index of the prompt nonthermal emission from $F \propto t^{-2.0}$ to $F_{\rm X} \propto t^{-1.1}$. If this scenario were true, the rotation period would evolve as $P \sim 10(t/\tau)^{1/2}$ ms and become $P \sim 1$ s at $t \sim 1$ yr. If a giant flare were to occur at this magnetar, such as the soft gamma-ray repeater (SGR) 1806-20 (Hurley et al. 2005), this would be clear evidence for our proposal.

The emission mechanism of the prompt nonthermal emission remains unclear. Ghisellini et al. (2007) have drawn the deabsorbed νF_ν spectrum from the *Swift* Ultraviolet/Optical Telescope (UVOT) data and argued that the extrapolation of the nonthermal spectrum with a constant low-energy photon index to the optical band joins with the detected thermal optical flux. This implies that the nonthermal spectrum does not extend below $\sim 10^{15}$ Hz. If this cutoff is due to the synchrotron self-absorption in the emitting shell with the isotropic kinetic energy $L_{\rm iso} \sim 10^{47}$ erg s^{-1} and the bulk Lorentz factor $\Gamma_0 \simeq 5$, the emission radius of the nonthermal emission is estimated as $r_0 \sim 10^{12}$ cm. It is less than the deceleration radius of the afterglow shell, estimated by $r_{\rm dec} \simeq 4\Gamma_0^2 c t_{\rm dec} \simeq 2 \times 10^{16}$ cm in our jet model. This implies that the prompt nonthermal emission may be produced by the internal dissipation of the jet. Ghisellini et al. (2007) have shown that a synchrotron inverse-Compton model could reproduce the prompt nonthermal emission, the anomalous X-ray afterglow, and the UV/optical thermal component, using parameters similar to those we suggest in this paper: $\Gamma_0 = 5$, $\theta_0 = 0.2$, and $r_0 = 7 \times 10^{11}$ cm.

The origins of the thermal components of this event are also unclear. A possible candidate is the emission from the expanding cocoon, as suggested by Fan et al. (2006) and Ghisellini et al. (2007; see also Ramirez-Ruiz et al. 2002). Within the hot jet model discussed in § 4, the energy deposited into the cocoon by the breakout time is estimated by $L_j t_{\rm br} \sim 3 \times 10^{47}$ erg, which is smaller than the energy of the detected thermal emission, $\gtrsim 10^{49}$ erg. The rest energy in the cocoon is estimated by $Mc^2\theta_{\rm br}^2/4 \sim 10^{49}$ erg, so the cocoon expansion velocity becomes $\beta_c \sim 10^{-1}$ outside the star. The cocoon shell catches up with the afterglow shell at $t \sim r_{\rm dec}/c\beta_c \sim 10^7$ s, and thus the cocoon energy will not affect the radio afterglow. The thermal components are detected in the X-ray band at $t \lesssim 10^4$ s and in the UV/optical band at $10^4 \lesssim t \lesssim 10^5$ s. To explain such behavior is an interesting future problem.

We appreciate the comments from the referee. We thank A. Mizuta, K. Murase, and N. Kawanaka for useful discussions. This work is supported in part by Grant-in-Aid for the 21st Century COE Center for Diversity and Universality in Physics from the Ministry of Education, Culture, Sports, Science, and Technology (MEXT) of Japan. K. T. was supported by the JSPS Research Fellowship for Young Scientists, grant 182666. K. I. was supported by Grant-in-Aid (18740147) from the MEXT of Japan. T. S. was supported by an appointment of the NASA Postdoctoral Program at the Goddard Space Flight Center, administered by Oak Ridge Associated Universities through a contract with NASA.

REFERENCES

Aloy, M. A., Müller, E., Ibáñez, J. M., Martí, J. M., & MacFadyen, A. 2000, ApJ, 531, L119
Amati, L., Della Valle, M., Frontera, F., Malesani, D., Guidorzi, C., Montanari, E., & Pian, E. 2007, A&A, 463, 913
Amati, L., et al. 2002, A&A, 390, 81
Barthelmy, S. D., et al. 2005, Space Sci. Rev., 120, 143
Begelman, M., & Cioffi, D. F. 1989, ApJ, 345, L21
Borgonovo, L., & Ryde, F. 2001, ApJ, 548, 770
Burrows, D. N., et al. 2005a, Science, 309, 1833
———. 2005b, Space Sci. Rev., 120, 165
Butler, N. R. 2007, ApJ, 656, 1001
Campana, S., et al. 2006, Nature, 442, 1008
Cappellaro, E., Evans, R., & Turatto, M. 1999, A&A, 351, 459
Chevalier, R. A., & Li, Z. Y. 1999, ApJ, 520, L29
Cobb, B. E., Bailyn, C. D., van Dokkum, P. G., & Natarajan, P. 2006, ApJ, 645, L113
Colgate, S. A. 1974, ApJ, 187, 333
Dahlen, T., et al. 2004, ApJ, 613, 189
Dai, Z. G., Zhang, B., & Liang, E. W. 2007, ApJ, submitted (astro-ph/0604510)
Daigne, F., & Mochkovitch, R. 2002, MNRAS, 336, 1271
Dermer, C. 2004, ApJ, 614, 284
Dyks, J., Zhang, B., & Fan, Y. Z. 2006, ApJ, submitted (astro-ph/0511699)
Fan, Y. Z., & Piran, T. 2006, MNRAS, 369, 197
Fan, Y. Z., Piran, T., & Xu, D. 2006, J. Cosmol. Astropart. Phys., 9, 13
Fenimore, E., Madras, C. D., & Nayakshin, S. 1996, ApJ, 473, 998
Ferrero, P., et al. 2006, A&A, 457, 857
Frail, D. A., Waxman, E., & Kulkarni, S. R. 2000, ApJ, 537, 191
Gehrels, N., et al. 2004, ApJ, 611, 1005
———. 2006, Nature, 444, 1044
Ghirlanda, G., Ghisellini, G., & Lazzati, D. 2004, ApJ, 616, 331
Ghisellini, G., Ghirlanda, G., Mereghetti, S., Bosnjak, Z., Tavecchio, F., & Firmani, C. 2006, MNRAS, 372, 1699
Ghisellini, G., Ghirlanda, G., & Tavecchio, F. 2007, MNRAS, 375, L36
Gorosabel, J., et al. 2006, A&A, 459, L33
Granot, J., Königl, A., & Piran, T. 2006, MNRAS, 370, 1946
Granot, J., Piran, T., & Sari, R. 1999, ApJ, 513, 679
Granot, J., Ramirez-Ruiz, E., & Perna, R. 2005, ApJ, 630, 1003
Guetta, D., Perna, R., Stella, L., & Vietri, M. 2004, ApJ, 615, L73
Gupta, N., & Zhang, B. 2007, Astropart. Phys., in press (astro-ph/0606744)
Harrison, F. A., et al. 1999, ApJ, 523, L121
Hurley, K., et al. 2005, Nature, 434, 1098
Ioka, K., Kobayashi, S., & Zhang, B. 2005, ApJ, 631, 429
Ioka, K., & Nakamura, T. 2001, ApJ, 554, L163
Ioka, K., Toma, K., Yamazaki, R., & Nakamura, T. 2006, A&A, 458, 7
Kaneko, Y., et al. 2007, ApJ, 654, 385
Kobayashi, S., & Zhang, B. 2007, ApJ, 655, 973
Kouveliotou, C., et al. 1998, Nature, 393, 235
Kumar, P., & Panaitescu, Z. 2000, ApJ, 541, L51
Lazzati, D., & Begelman, M. C. 2005, ApJ, 629, 903
———. 2006, ApJ, 641, 972
Li, L. X. 2007, MNRAS, 375, 240
Liang, E. W., Zhang, B., Virgili, F., & Dai, Z. G. 2006a, ApJ, submitted (astro-ph/0605200)
Liang, E. W., Zhang, B., Zhang, B. B., & Dai, Z. G. 2006b, preprint (astro-ph/0606565)
Liang, E. W., Zhang, B. B., Stamatikos, M., Zhang, B., Norris, J., Gehrels, N., Zhang, J., & Dai, Z. G. 2006c, ApJ, 653, L81
Liang, E. W., et al. 2006d, ApJ, 646, 351
Lithwick, Y., & Sari, R. 2001, ApJ, 555, 540
Livio, M., & Waxman, E. 2000, ApJ, 538, 187
Lloyd-Ronning, N. M., & Zhang, B. 2004, ApJ, 613, 477
MacFadyen, A. I., & Woosley, S. E. 1999, ApJ, 524, 262
Markwardt, C. B., et al. 2005, ApJ, 633, L77
Matzner, C. D. 2003, MNRAS, 345, 575
Matzner, C. D., & McKee, C. F. 1999, ApJ, 510, 379
Mazzali, P. A., Deng, J., Nomoto, K., Pian, E., Tominaga, N., Tanaka, M., & Maeda, K. 2006, Nature, 442, 1018
Mészáros, P. 2006, Rep. Prog. Phys., 69, 2259
Mészáros, P., & Rees, M. J. 2001, ApJ, 556, L37
Mirabal, N., Halpern, J. P., An, D., Thorstensen, J. R., & Terndrup, D. M. 2006, ApJ, 643, L99
Mizuta, A., Yamasaki, T., Nagataki, S., & Mineshige, S. 2006, ApJ, 651, 960
Modjaz, M., et al. 2006, ApJ, 645, L21
Murase, K., Ioka, K., Nagataki, S., & Nakamura, T. 2006, ApJ, 651, L5
O'Brien, P. T., et al. 2006, ApJ, 647, 1213
Paczyński, B., & Rhoads, J. E. 1993, ApJ, 418, L5
Panaitescu, A., & Kumar, P. 2002, ApJ, 571, 779
Pian, E., et al. 2006, Nature, 442, 1011
Piran, T. 2005, Rev. Mod. Phys., 76, 1143
Preece, R. D., Brrigs, M. S., Mallozzi, R. S., Pendleton, G. N., Paciesas, W. S., & Band, D. L. 2000, ApJS, 126, 19
Ramirez-Ruiz, E., Celotti, A., & Rees, M. J. 2002, MNRAS, 337, 1349
Ramirez-Ruiz, E., Granot, J., Kouveliotou, C., Woosley, S. E., Patel, S. K., & Mazzali, P. A. 2005, ApJ, 625, L91
Rees, M. J., & Mészáros, P. 1992, MNRAS, 258, P41
Rhoads, J. E. 1999, ApJ, 525, 737
Rossi, E., Lazzati, D., & Rees, M. J. 2002, MNRAS, 332, 945
Rybicki, G. B., & Lightman, A. P. 1979, Radiation Processes in Astrophysics (New York: Wiley)
Ryde, F., & Petrosian, V. 2002, ApJ, 578, 290
Sakamoto, T., et al. 2005, ApJ, 629, 311
Sari, R., & Piran, T. 1997, MNRAS, 287, 110
Sari, R., Piran, T., & Halpern, J. P. 1999, ApJ, 519, L17
Sari, R., Piran, T., & Narayan, R. 1998, ApJ, 497, L17
Shapiro, S. L., & Teukolsky, S. A. 1983, Black Holes, White Dwarfs, and Neutron Stars: The Physics of Compact Objects (New York: Wiley)
Soderberg, A. M., et al. 2006, Nature, 442, 1014
Sollerman, J., et al. 2006, A&A, 454, 503
Stanek, K. Z., et al. 2006, Acta Astron., 56, 333
Stratta, G., et al. 2007, A&A, 461, 485
Tan, J. C., Matzner, C. D., & McKee, C. F. 2001, ApJ, 551, 946
Toma, K., Ioka, K., Yamazaki, R., & Nakamura, T. 2006, ApJ, 640, L139
Toma, K., Yamazaki, R., & Nakamura, T. 2005, ApJ, 635, 481
Umeda, H., Tominaga, N., Maeda, K., & Nomoto, K. 2005, ApJ, 633, L17
Wang, X. Y., Li, Z., Waxman, E., & Mészáros, P. 2006, ApJ, submitted (astro-ph/0608033)
Waxman, E., & Mészáros, P. 2003, ApJ, 584, 390
Woosley, S. E. 1993, ApJ, 405, 273
Woosley, S. E., & Bloom, J. S. 2006, ARA&A, 44, 507
Yamazaki, R., Toma, K., Ioka, K., & Nakamura, T. 2006, MNRAS, 369, 311
Yamazaki, R., Yonetoku, D., & Nakamura, T. 2003, ApJ, 594, L79
Yost, S. A., Harrison, F. A., Sari, R., & Frail, D. A. 2003, ApJ, 597, 459
Zhang, B., Fan, Y. Z., Dyks, J., Kobayashi, S., Mészáros, P., Burrows, D. N., Nousek, J. A., & Gehrels, N. 2006, ApJ, 642, 354
Zhang, B., & Mészáros, P. 2002, ApJ, 571, 876
———. 2004, Int. J. Mod. Phys. A, 19, 2385
Zhang, B., et al. 2007, ApJ, 655, 989
Zhang, W., Woosley, S. E., & Heger, A. 2004, ApJ, 608, 365
Zhang, W., Woosley, S. E., & MacFadyen, A. I. 2003, ApJ, 586, 356